

INFRARED THERMAL IMAGING DETECTION OF DEBONDING DEFECTS IN CARBON FIBER REINFORCED POLYMER BASED ON PULSED THERMAL WAVE EXCITATION

by

**Chi-Wu BU^{a*}, Bo ZHAO^a, Tao LIU^a, Guo-Zeng LIU^a,
Chang-Yu LIAO^a, and Qing-Ju TANG^b**

^a College of Light Industry, Harbin University of Commerce, Harbin, China

^b School of Mechanical Engineering, Heilongjiang University of Science and Technology, Harbin, China

Original scientific paper
<https://doi.org/10.2298/TSCI2006887B>

The carbon fiber reinforced composite has been widely used in many fields of the aviation industry due to the good resistance to fatigue damage, impact resistance, and easy processing. Firstly, the pulse heat conduction model of the carbon fiber reinforced composite is established, and the simulation experiment is completed based on the customized specimen with the defects. The influences of the thermal excitation power and pulse width on the defect detection effect are analyzed and obtained. The total harmonic distortion algorithm is used to process the experimental image sequence. The simulation and experimental results are compared and analyzed to verify their unity. It may provide the theoretical basis and empirical guidance for the defect detection of the composite materials.

Key words: *carbon fiber reinforced composite, total harmonic distortion, infrared thermal imaging, defect detection*

Introduction

The carbon fiber reinforced polymer (CFRP) has been used to produce a variety of aircraft components, including doors and clamps, as well as wing flaps and bodies. The demanding application is associated with superior properties of CFRP, such as high strength and stiffness, low weight and high fatigue resistance. However, serious damage, especially debonding defects, often occurs during the service. Debonding will not only reduce the integrity of the structure, but also seriously reduce its bearing capacity [1, 2]. Therefore, it is necessary to carry out nondestructive testing of CFRP debonding defects. As a new non-destructive testing technology, infrared thermography has been developed rapidly in recent years [3]. According to the different heating modes, the infrared thermal imaging includes pulse thermal (PT) method [4, 5], lock-in method [6, 7], and linear frequency modulation method [8, 9]. The PT method has the advantages of fast detection, convenient on-line detection and so on.

The target of the present paper is to show that the finite element simulation and experimental research are combined to study the debonding defects detection of the CFRP specimen, and the influence of pulse excitation on the detection effect under different power and pulse width is analyzed.

* Corresponding author, e-mail: buchuwu@126.com

Theory analysis

Pulsed infrared thermal wave imaging technology uses pulse signal to excite the surface of the specimen, and the thermal wave propagates to the interior of the specimen. The defects in the specimen will affect the propagation of the thermal wave and cause the change of the temperature field on the surface of the specimen. The infrared thermal image sequence is collected and recorded by the infrared thermal camera. Finally, the infrared thermal image sequence is analyzed and processed to realize the detection and evaluation of defects.

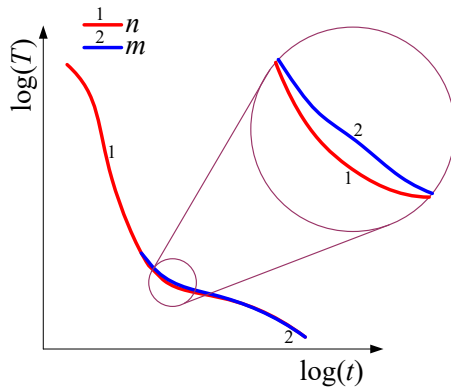


Figure 1. Attenuation curve of pulse excitation temperature in logarithmic domain

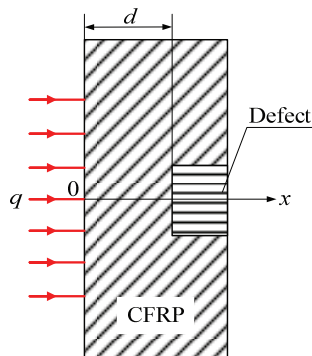


Figure 2. Heat transfer schematic diagram of CFRP

The purpose of damage detection is to classify pixels according to cooling behavior. Figure 1 shows two typical observed temperature decay curves of n point (1) and m point (2) in frequency domain [10]. Under the action of external thermal excitation, the heat flow is conducted inside the CFRP, the heat transfer principle is shown in fig. 2, where, d is the depth of defect and q – the heat flow loaded on surface of the CFRP specimen.

The 3-D heat conduction equation is given [11]:

$$\frac{\partial^2 T}{\partial x^2} + \frac{\partial^2 T}{\partial y^2} + \frac{\partial^2 T}{\partial z^2} + \frac{q}{k} = \frac{1}{\alpha} \frac{\partial T}{\partial t} \quad (1)$$

$$\alpha = \frac{k}{\rho c} \quad (2)$$

where α is the thermal diffusion coefficient, k – the thermal conductivity, ρ – the density, c – the specific heat capacity, and q – the heat flow.

In the 1-D case, the heat conduction equation is rewritten:

$$\frac{\partial^2 T(x,t)}{\partial x^2} - \frac{1}{\alpha} \frac{\partial T(x,t)}{\partial t} = -\frac{q(x,t)}{k} \quad (3)$$

Uniforming the plane pulse, the heat source, used in this test, is given:

$$q(x,t) = Q\delta(x)\delta(t) \quad (4)$$

where Q is heat flux. If the 1-D heat conduction is considered and the surface of the object completely absorbs the energy from the heat source without considering the diffusion loss, then eq. (4) reads:

$$k \frac{\partial^2 T(x,t)}{\partial x^2} - \rho c \frac{\partial T(x,t)}{\partial t} = -Q\delta(x)\delta(t) \quad (5)$$

The boundary conditions are given:

$$\left[\frac{\partial T(x,t)}{\partial x} \right]_{x=0, t=0} = 0 \quad (6)$$

$$\left[\frac{\partial T(x,t)}{\partial x} \right]_{x=d, t=0} = 0 \quad (7)$$

The relationship between temperature, depth and time can be given:

$$T(x,t) = \frac{Q}{\sqrt{\pi k c \rho t}} e^{-\frac{x^2}{4\alpha t}} \quad (8)$$

The temperature difference, denoted as ΔT , between the defective and defect-free areas can be expressed:

$$\Delta T = \frac{Q}{\sqrt{\pi k c \rho t}} - \frac{Q}{\sqrt{\pi k c \rho t}} e^{-\frac{d^2}{4\alpha t}} = \frac{Q}{\sqrt{\pi k c \rho t}} \left(1 - e^{-\frac{d^2}{4\alpha t}} \right) \quad (9)$$

Numerical simulation

Establishment of finite element model

The geometric size of the tested CFRP specimen is 100 mm × 100 mm × 4 mm, and the artificial defects of different size are distributed as shown in fig. 3. The thermophysical parameters are shown in tab. 1.

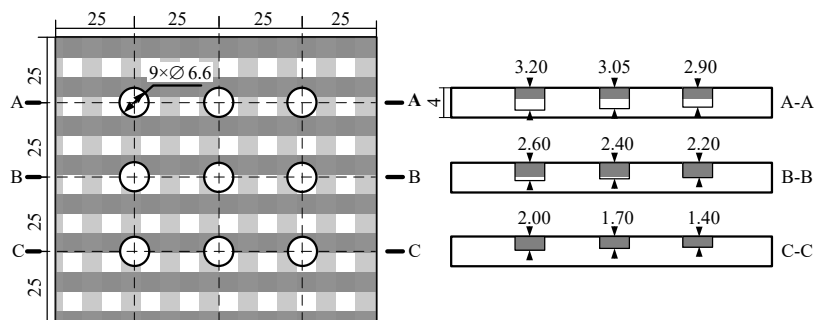


Figure 3. Distribution of geometric location of defects in the specimen

Table 1. Thermophysical parameters

| Material | Thermal conductivity [Wm ⁻¹ K ⁻¹] | Density [kgm ⁻³] | Specific heat capacity [Jkg ⁻¹ K ⁻¹] |
|--------------|--|------------------------------|---|
| Epoxy resin | 0.251 | 2170 | 740 |
| Carbon fibre | 4.18 | 1550 | 793 |

Simulation experiments and result analysis

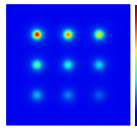
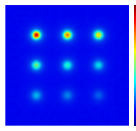
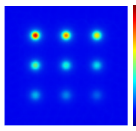
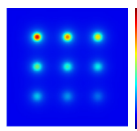
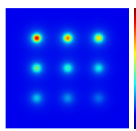
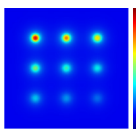
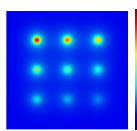
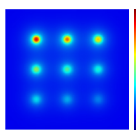
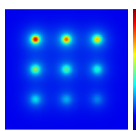
In the simulation experiments, the initial temperature, heat transfer coefficient, sampling frequency, and heating time were set as 293.15 K, 10 W/m²K, 30 Hz, and 20 seconds, respectively. Three different heat flux P of 800 W/m², 1200 W/m², and 1600 W/m² was loaded on the top surface of the specimen, and the pulse width B was set as 1, 3, and 5 seconds for orthogonal analysis. The maximum temperature difference $\Delta T_{\max}(t)$ is defined:

$$\Delta T_{\max}(t) = T_2(t) - T_1(t) \quad (12)$$

where $T_2(t)$ is the maximum temperature value of the specimen surface at time t , which is usually the temperature value of the defect center point with large diameter and depth, and $T_1(t)$ is the minimum surface temperature of the specimen, which is usually the temperature value of the defect free area.

Table 2 shows the temperature distribution under different heat flux, P , and pulse width B . It can be seen that in the heating stage, with the increase of P and B , the defect contour is becoming more and more clearer; The maximum temperature difference $\Delta T_{\max}(t)$ also increases with the increase of P and B , and the defect contour is the most clear when $P = 1600 \text{ W/m}^2$ and $B = 5$ seconds.

Table 2. Temperature distribution under different heat flux and pulse width

| $B \backslash P$ | 800 W/m ² | 1200 W/m ² | 1600 W/m ² |
|------------------|---|---|--|
| 1 [s] |  $\Delta T_{\max} = 1.04 \text{ K}$ |  $\Delta T_{\max} = 1.57 \text{ K}$ |  $\Delta T_{\max} = 2.09 \text{ K}$ |
| 3 [s] |  $\Delta T_{\max} = 2.04 \text{ K}$ |  $\Delta T_{\max} = 3.05 \text{ K}$ |  $\Delta T_{\max} = 4.06 \text{ K}$ |
| 5 [s] |  $\Delta T_{\max} = 2.25 \text{ K}$ |  $\Delta T_{\max} = 3.37 \text{ K}$ |  $\Delta T_{\max} = 4.49 \text{ K}$ |

Experimental study

The aforementioned simulation results show that the ideal detection results are obtained when $P = 1600 \text{ W/m}^2$ and $B = 5$ seconds. So, two sets of the experiments under the optimized parameters were carried out on the built infrared thermal wave testing system. The infrared camera is FLIR A655sc. The sampling frequency and sampling time was set as 30 Hz and 20 seconds, respectively.

In the process of infrared image imaging, the captured infrared image sequence is usually with high noise and low contrast due to the interference of uneven heating and infrared radiation of surrounding environment. So, in order to improve the signal-to-noise ratio (SNR), background reduction and total harmonic distortion [12] algorithms were applied to process the image sequences, and normalization treatment was expressed by [13]:

$$Z_n = \frac{Z - Z_{\min}}{Z_{\max} - Z_{\min}} \quad (13)$$

where Z_n is the normalized value, Z – the value after background reduction, both Z_{\max} and Z_{\min} are the maximum and minimum values of Z , respectively.

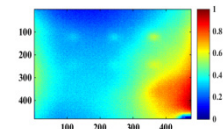
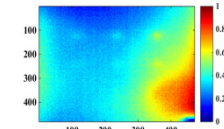
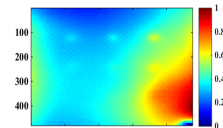
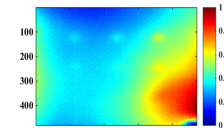
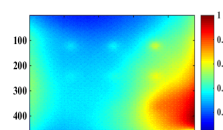
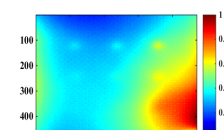
The SNR_D was selected to measure the influence of different parameters on the processed infrared image, given:

$$SNR_D = \frac{|T - R|}{\sigma^2} \quad (14)$$

where SNR_D is the SNR of defects, σ^2 – the standard deviation of the defective area, R – the temperature of the reference area, and T – the temperature of the defective area.

Table 3 shows the characteristic images and their SNR_D of the image sequences obtained under different experimental parameters after being processed by the above algorithm. It can be seen from tab. 3 that when the pulse width is constant, as the heat flux increases, the SNR_D increases gradually, and the contrast between the defect and defect-free area is more obvious, which shows that the increase of the loaded heat flux is beneficial to the identification of the defect. When the heat flux density is constant, as the pulse width increases and the SNR_D ratio increases gradually, which show that the increase of the pulse is beneficial to the identification of the defects. The test and simulation results are consistent in trend.

Table 3. Comparison of different parameters

| | The processed image | SNR_D | | The processed image | SNR_D |
|-------------|---|---------|--------------------------|---|---------|
| $B = 5$ [s] |  $P = 800 \text{ W/m}^2$ | 25.46 | $P = 1600 \text{ W/m}^2$ |  $B = 1$ [s] | 33.77 |
| |  $P = 1200 \text{ W/m}^2$ | 30.28 | |  $B = 3$ [s] | 38.37 |
| |  $P = 1600 \text{ W/m}^2$ | 36.55 | |  $B = 5$ [s] | 41.72 |

Conclusion

In the present work, the infrared thermal imaging detection of debonding defects in CFRP has been carried out based on pulsed thermal wave excitation. The influence law of heat flux and pulse width on defect recognition was arrived. With the increasing of heat flux and pulse width, the SNR_D and defect recognition effect can be improved. Compared with the pulse width, the heat flux has the more significant influence on SNR_D and the defect recognition effect.

Acknowledgment

This project is supported by National Natural Science Foundation of China (Grant No. 51775175), Heilongjiang Science and Technology Plan Provincial Hospital Science and

Technology Cooperation Project (Grant No. YS18A18), and Heilongjiang Province Natural Science Fund (Grant No. E2018050).

Nomenclature

c – specific heat capacity, [$\text{Jkg}^{-1}\text{K}^{-1}$]
 Q – heat of outflow, [J]
 SNR – signal-to-noise ratio, [–]
 T – temperature distribution, [K]
 t – time, [s]

Greek symbols

α – thermal diffusion coefficient, [–]
 δ – plane pulse
 ρ – material density, [kgm^{-3}]

References

- [1] Hauschwitz, P., *et al.*, Fabrication of Functional Superhydrophobic Surfaces on Carbon Fibre Reinforced Plastics by IR and UV Direct Laser Interference Patterning, *Applied Surface Science*, 508 (2020), Apr., pp. 144817
- [2] Shi, Y., *et al.*, Effects of Inkjet Printed Toughener on Delamination Suppression in Drilling of Carbon Fibre Reinforced Plastics (CFRPs), *Composite Structures*, 245 (2020), Aug., pp.112339
- [3] Wang, H., *et al.*, Phase-Locked Restored Pseudo Heat Flux Thermography for Detecting Delamination Inside Carbon Fiber Reinforced Composites, *IEEE Transactions on Industrial Informatics*, 15 (2018), 5, pp. 2938-2946
- [4] Henrique, F., *et al.*, Carbon Fiber Composites Inspection and Defect Characterization Using Active Infrared Thermography: Numerical Simulations and Experimental Results, *Applied optics*, 55 (2016), 34, pp. 46-53
- [5] Bu, C., *et al.*, Quantitative Detection of Thermal Barrier Coating Thickness based on Simulated Annealing Algorithm using Pulsed Infrared Thermography Technology, *Applied Thermal Engineering*, 99 (2016), Apr., pp. 751-755
- [6] Palumbo, D., *et al.*, Ultrasonic Analysis and Lock-in Thermography for Debonding Evaluation of Composite Adhesive Joints, *Ndt & E International*, 78 (2016), 3, pp. 1-9
- [7] Montanini, R., Quantitative Determination of Subsurface Defects in a Reference Sample Made of Plexiglas by Means of Lock-in and Pulse Phase Infrared Thermography, *Infrared Physics & Technology*, 53 (2010), 5, pp. 363-371
- [8] Laureti, S., *et al.*, Comparative Study between Linear and Non-linear Frequency-modulated Pulse-Compression Thermography, *Applied optics*, 57 (2018), 18, pp. 32-39
- [9] Massaro, R. D., *et al.*, A Comparative Study between Frequency-Modulated Continuous Wave LADAR and Linear LiDAR, *International Archives of the Photogrammetry Remote Sensing & S, XL-1* (2014), Nov., pp. 233-239
- [10] Sirikham, A., *et al.*, Estimation of Damage Thickness in Fiber-Reinforced Composites using Pulsed Thermography, *IEEE Transactions on Industrial Informatics*, 15 (2019), 1, pp. 445-453
- [11] He, Y., *et al.*, Dynamic Scanning Electromagnetic Infrared Thermographic Analysis based on Blind Source Separation for Industrial Metallic Damage Evaluation, *IEEE Transactions on Industrial Informatics*, 14 (2018), 12, pp. 5610-5619
- [12] Nayebi, V., *et al.*, New Method for High Impedance Faults Detection Using Total Harmonic Distortion Properties and Time Variations of Current Waveform, *International Journal of Automation & Power Engineering*, 1 (2012), 7, pp. 165-173
- [13] Bu, C., *et al.*, Debonding Defects Detection of FMLs based on Long Pulsed Infrared Thermography Technique, *Infrared Physics & Technology*, 104 (2020), Jan., pp.103074
- [14] Wei, J., *et al.*, A Laser Arrays Scan Thermography (LAsST) for the Rapid Inspection of CFRP Composite with Subsurface Defects, *Composite Structures*, 226 (2019), pp.111201